Thermal conductivity of silicene calculated using an optimized Stillinger-Weber potential

Xiaoliang Zhang,[1] Han Xie,[2] Ming Hu,[1,3,*] Hua Bao,[2,*] Shengying Yue,[4] Guangzhao Qin,[4] and Gang Su[4]

[1]*Institute of Mineral Engineering, Division of Materials Science and Engineering, Faculty of Georesources and Materials Engineering, Rheinisch-Westfaelische Technische Hochschule (RWTH) Aachen University, 52064 Aachen, Germany*

[2]*University of Michigan–Shanghai Jiao Tong University Joint Institute, Shanghai Jiao Tong University, Shanghai, China 200240*

[3]*Aachen Institute for Advanced Study in Computational Engineering Science (AICES), RWTH Aachen University, 52062 Aachen, Germany*

[4]*Theoretical Condensed Matter Physics and Computational Materials Physics Laboratory, School of Physics, University of Chinese Academy of Science, Beijing, China 100049*

(Received 25 November 2013; revised manuscript received 5 February 2014; published 26 February 2014)

Silicene, the silicon-based counterpart of graphene with a two-dimensional honeycomb lattice, has attracted tremendous interest both theoretically and experimentally due to its significant potential industrial applications. From the aspect of theoretical study, the widely used classical molecular dynamics simulation is an appropriate way to investigate the transport phenomena and mechanisms in nanostructures such as silicene. Unfortunately, no available interatomic potential can precisely characterize the unique features of silicene. Here, we optimized the Stillinger-Weber potential parameters specifically for a single-layer Si sheet, which can accurately reproduce the low buckling structure of silicene and the full phonon dispersion curves obtained from *ab initio* calculations. By performing equilibrium and nonequilibrium molecular dynamics simulations and anharmonic lattice dynamics calculations with the new potential, we reveal that the three methods consistently yield an extremely low thermal conductivity of silicene and a short phonon mean-free path, suggesting silicene as a potential candidate for high-efficiency thermoelectric materials. Moreover, by qualifying the relative contributions of lattice vibrations in different directions, we found that the longitudinal phonon modes dominate the thermal transport in silicene, which is fundamentally different from graphene, despite the similarity of their two-dimensional honeycomb lattices.

DOI: 10.1103/PhysRevB.89.054310 PACS number(s): 66.70.−f, 63.22.Np, 65.80.−g

I. INTRODUCTION

Graphene, as the first two-dimensional atomic crystal available to us, possesses extreme mechanical strength, exceptionally high electrical and thermal conductivities, as well as many other supreme properties, all of which make it highly attractive for numerous applications [1]. Inspired by the prospective properties of graphene, there has been increasing interest in investigating other two-dimensional honeycomb lattices, for example, silicene. Actually, silicene—the silicon counterpart of graphene—also has a two-dimensional structure that leads to a host of interesting physical and chemical properties of significant utility [2–5]. In particular, in terms of thermoelectric application, silicene is even more exciting than graphene. Graphene has been reported to possess the highest intrinsic limit of electrical mobility at room temperature [6], which is a good motivation for thermoelectric applications. However, the experimentally measured thermal conductivity of suspended single-layer graphene is reported to be as high as $\sim(4.84 \pm 0.44) \times 10^3$ to $(5.30 \pm 0.48) \times 10^3$ W/mK at room temperature [7], which is almost the highest thermal conductivity of the existing materials. Although the extremely high thermal conductivity is useful for heat dissipation in electronics, it hinders graphene as an efficient thermoelectric material, because energy conversion efficiency is inversely proportional to the thermal conductivity. Even worse, the Seebeck coefficient of graphene is very small due to its zero band gap [8]. Silicene, however, may be very promising for thermoelectric energy conversion. First of all, from an electronic structure point of view, *ab initio* calculations suggest that silicene is equivalent to graphene [9], i.e., the electrical conductivity of silicene is as high as that of graphene. Second, in contrast to graphene, silicene has a buckled atomic structure, leading to a nonzero energy gap and enhanced Seebeck coefficient [10]. Therefore, there is an urgent demand to quantify the thermal transport property of silicene.

In addition to thermoelectric applications, silicene, with supreme electronic properties similar to those of graphene, has also shown great potential for other applications, such as nanoelectronics [11–13]. More importantly, compared to graphene, silicene is more easily integrated with existing silicon-based electronic devices and technologies.

Experimental studies on the physical properties of silicene are recent, and many important mechanisms have not been explored due to the technical challenges for experimental scientists. From the aspect of theoretical study, the widely used classical molecular dynamics simulation is an appropriate way to investigate the transport phenomena and mechanisms in nanostructures such as silicene. Unfortunately, we found that no available interatomic potential can precisely characterize the unique features of silicene, e.g., reproducing the low buckling structure and the corresponding buckling distance confirmed by both experiments [14] and *ab initio* calculations [15]. Even worse, the widely used Stillinger-Weber (SW) potential [16] cannot maintain the hexagonal structure of the single-layer Si sheet. Therefore, it is necessary to develop a new set of empirical potentials to be used in the molecular dynamics simulation [17]. Tersoff [18,19] and SW potentials [16] have been extensively used to investigate the silicon-based materials, which can be used as candidates for parameter optimization for silicene. Compared with the Tersoff potential, the SW potential has a simpler form and fewer parameters to

*Author to whom correspondence should be addressed. hum@ghi.rwth-aachen.de or hua.bao@sjtu.edu.cn

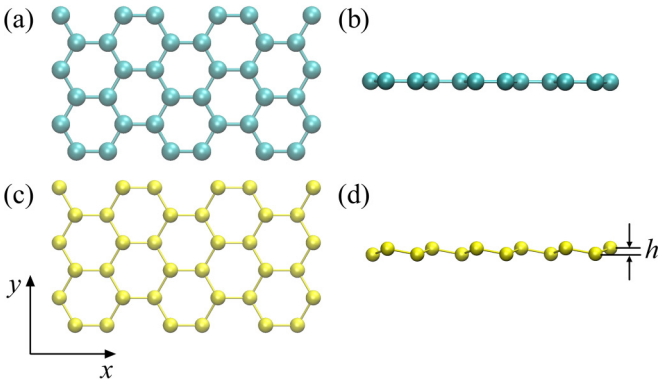

FIG. 1. (Color online) Comparison of the crystal structures between graphene and silicene. (a) Top view and (b) side view of graphene. (c) Top view and (d) side view of silicene. The graphene has perfect planar structure, while silicene has a low buckling in out-of-plane direction (buckling distance indicated by h).

fit, so it is faster and more appropriate for parameter fitting. Based on the advantages above, we choose the SW potential model for silicene.

In this paper, we present new SW potential parameters optimized for silicene, which reproduce the buckling structure and full phonon dispersion curves from *ab initio* calculations. We further perform detailed investigations of the lattice thermal conductivity of silicene using our optimized SW potentials. In Sec. II, we briefly describe the approach of parameter optimization and present the optimized SW parameters. In Sec. III, we report the lattice thermal conductivity of silicene using the fitted SW parameters by equilibrium molecular dynamics (EMD) and nonequilibrium molecular dynamics (NEMD) simulations and by the anharmonic lattice dynamics (ALD) method. In Sec. IV, we further analyze the contributions to lattice thermal conductivity from each normal mode and from different vibrational directions. In Sec. V, we present a summary and conclusion.

II. PARAMETER OPTIMIZATION

The *ab initio* calculation is first carried out using the Quantum ESPRESSO package [20]. The Perdew-Zunger [21] local density approximation is chosen for the exchange-correlation functional, and the norm-conserving pseudopotential [22] is used. The calculation is performed with a unit cell containing two silicon atoms. The height of the cell is larger than 10 Å to avoid the interaction between different layers. A $16 \times 16 \times 1$ k-point mesh is used for the Brillouin zone integration. Geometry optimization is performed until the force on each atom is smaller than 0.0257 eV/Å (0.001 Ry/Bohr). Here, our *ab initio* calculation shows that the bond length is 2.2420 Å, and the buckling distance is 0.4269 Å, which is comparable with previous *ab initio* simulations [23,24]. The optimized crystal structure of silicene from *ab initio* calculations is shown in Fig. 1, together with the graphene structure. Note that we did not consider the bond length difference between graphene and silicene in Fig. 1. It can be seen that both graphene and silicene are hexagonal honeycomb lattices, and the major difference between silicene and graphene is the buckling distance (h). For graphene, $h = 0$; while for silicene, h=0.4269 Å. Note that there are also other reported values for the buckling distance, ranging from 0.02 to 0.046 nm [23–26]. For silicene, the low buckling structure and the corresponding buckling distance h is an important physical quantity to fit.

TABLE I. Two sets of optimized SW parameters for silicene (see text for different fitting strategies). For units, ε is in electron volts, and σ is in angstroms. The rest parameters are dimensionless.

	Original SW	Optimized SW1	Optimized SW2
ε (eV)	2.1683	2.1683	2.1683
σ (Å)	2.0951	2.00336	1.99751
a	1.8	1.774753	1.8
λ	21.0	15.662962	22.275515
γ	1.2	1.181855	1.2
$\cos(\theta_0)$	−0.333333333333	−0.44561015	−0.44561011
A	7.049556277	6.0	5.834064
B	0.6022245584	0.618328	0.602225
p	4	4	4
q	0	0	0
tol	0	0	0

For a thermal transport study by classical potential, phonons are assumed to be the most important energy carriers, and phonon dispersion is of great significance for the investigation of thermal transport. Thus, we also focus on fitting the parameters for the phonon dispersion of silicene to the *ab initio* results, which is calculated with the density functional perturbation theory [27] implemented in the Quantum ESPRESSO package. The GULP [28] program was used to fit the SW potential parameters. The phonon frequencies of 31 k-points in the Brillouin zone along $\Gamma \rightarrow K \rightarrow M \rightarrow \Gamma$ are used as the target properties in the parameters fitting. In order to accelerate the convergence of the fitting procedure, we used the original SW potential [16] parameters as an initial guess.

The new SW potential parameters optimized for silicene are given in Table I, as compared with original values. Note that we present two sets of optimized SW parameters, namely, optimized SW1 and optimized SW2, using different fitting strategies. The optimized SW1 parameters are fitted to *all* the phonon dispersion curves, and the optimized SW2 parameters are fitted to *only* the acoustic phonon dispersion curves. The *ab initio* phonon dispersion of silicene and the results calculated by the optimized SW1 and optimized SW2 parameters are compared in Fig. 2. We see that the overall the phonon dispersion curves are fitted quite well by the optimized SW1 parameters, and the optical phonon branches are perfectly reproduced. However, the acoustic phonon branches are better fitted by the optimized SW2 parameters than the optimized SW1 parameters, while the dispersion curves of optical phonons remain almost unchanged. Nevertheless, the buckling distance (0.4269 Å), bond length (2.2420 Å), and bond angle (116.46°) obtained from our *ab initio* calculations are precisely reproduced by both sets of optimized SW parameters.

III. THERMAL CONDUCTIVITY CALCULATION

Using the optimized SW potentials, we first performed both EMD and NEMD simulations using the LAMMPS [29]

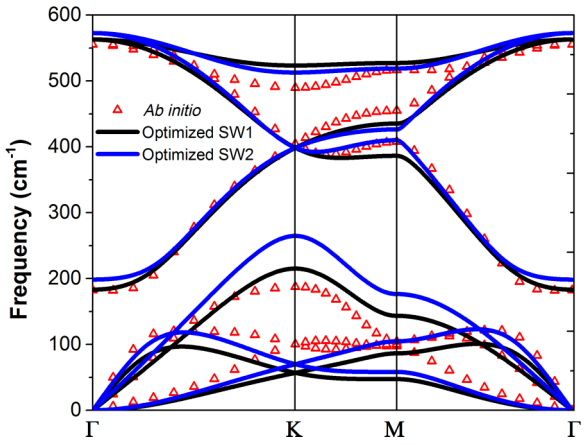

FIG. 2. (Color online) Full phonon dispersion curves of silicene in the Brillouin zone. The solid black and blue lines are calculated by the optimized SW1 and optimized SW2 parameters, respectively. The red triangles are the results from *ab initio* calculations.

package to calculate the thermal conductivity of silicene. In all simulations performed herein, a time step of 0.5 fs was used.

In the EMD simulation, periodic boundary conditions are used in the x and y directions (in-plane), and a free boundary condition is used in the z direction (out-of-plane). The thermal conductivity was estimated by the Green-Kubo method [30]

$$\kappa_{MD} = \frac{V}{3k_B T^2} \int \langle \vec{J}(0) \cdot \vec{J}(t) \rangle dt, \tag{1}$$

where V is volume, k_B is the Boltzmann constant, T is temperature, $\vec{J}$ is heat flux, and $\langle\rangle$ denotes the time average. The heat flux $\vec{J}$ was calculated by

$$\vec{J} = \frac{1}{V} \left[\sum_i E_i \vec{v}_i - \sum_i \vec{\vec{S}}_i \vec{v}_i \right], \tag{2}$$

where E_i is the total energy (kinetic and potential) of the atom i, $\vec{v}_i$ is the velocity of the atom i, and $\vec{\vec{S}}_i$ is the symmetric stress tensor of the atom i defined as [29]

$$\vec{\vec{S}} = \begin{bmatrix} S_{xx} & S_{xy} & S_{xz} \\ S_{xy} & S_{yy} & S_{yz} \\ S_{xz} & S_{yz} & S_{zz} \end{bmatrix}, \tag{3}$$

with

$$S_{\alpha\beta} = -\frac{1}{2} \sum_{n=1}^{N_2} (r_{1\alpha} f_{1\beta} + r_{2\alpha} f_{2\beta}) - \frac{1}{3} \sum_{n=1}^{N_3} (r_{1\alpha} f_{1\beta} + r_{2\alpha} f_{2\beta} + r_{3\alpha} f_{3\beta}), \tag{4}$$

where α and β denote the x, y, or z direction. The first and second terms in the definition of $S_{\alpha\beta}$ define the contribution from the two-body and three-body interactions, respectively. The thickness of silicene was chosen as 4.2 Å in calculating the system volume, equal to the van der Waals diameter of the Si atoms [5]. To achieve a good convergence for the thermal conductivity of silicene, we took every successive 0.5 ns of heat current data as different samples and calculated the thermal conductivities of these samples. Furthermore, using the method just described, we ran ten independent simulations with different initial atomic velocities. Typically, for each simulation, we used 50–500 ns of heat current data to calculate the thermal conductivity. We first calculated the average thermal conductivity of all the heat current samples in each simulation, and then the final thermal conductivity result was taken as the average over the ten runs for a correlation time between 20 and 50 ps.

In the NEMD simulation, the periodic boundary condition was used in the x (transverse) direction, and a free boundary condition was used in the z (out-of-plane) direction. We set 1-nm-long regions at both ends in the y (longitudinal) direction as a rigid wall. In the first stage of NEMD simulations, we relaxed the system at 300 K for 0.5 ns with the walls moving freely along the y direction, corresponding to zero pressure, using a Nosé-Hoover thermostat [31,32]. After NPT (constant particles, pressure, and temperature) relaxation, we froze the walls and continued to relax the system with the NPT ensemble for another 0.5 ns, and in this stage, we only allowed the system to relax in the x direction. After that, we continued to relax the system with the NVE (constant particles, volume and no thermostat) ensemble for another 0.5 ns. Following equilibration, we computed the thermal conductivity of the system using the NEMD method. It is well known that using the NEMD method to compute thermal conductivity relies on a steady heat flux, which must be established along the desired direction. Currently, to realize it, there are two different methods: (1) constant heat flux, e.g., the Jund and Jullien algorithm [33] or the Müller-Plathe algorithm [34] in which the heat current or flux is an input parameter and the resulting temperature gradient is calculated; and (2) constant temperature gradient, i.e., the heat source and heat sink are connected to constant temperature thermostats (thus, the temperature gradient is known in advance), and the resulting heat flux is calculated. In our simulation, we adopted the second method because for a constant heat flux method, the temperature difference in the model system cannot be easily estimated and usually the heat flux parameters must be tried many times to achieve an appropriate temperature difference. To establish a temperature gradient along the longitudinal direction, we set another 5-nm-long region next to the rigid wall as a heat source and heat sink. The temperature gradient is realized by using Nosé-Hoover thermostats to keep the temperature of heat source and heat sink at 320 and 280 K, respectively. To calculate the heat flux along the longitudinal direction, we record the input and output energy for the heat source and heat sink at each step, and the averaged heat power divided by the cross-sectional area is considered to be the heat flux. Again, the thickness of silicene was chosen as 4.2 Å in calculating the cross-sectional area [5].

The thermal conductivity of silicene from the NEMD is calculated by Fourier's law

$$\kappa_{\text{NEMD}} = -\frac{J_L}{\partial T / \partial y}, \tag{5}$$

where J_L is the averaged heat flux in the longitudinal direction and $\partial T/\partial y$ is the temperature gradient determined from a linear fitting of the time-averaged temperature profile along

the longitudinal (y) direction. We did not observe a noticeable nonlinear temperature profile due to the small temperature difference in our model system, so we used all the temperature data to calculate the temperature gradient. A typical heat-source heat-sink run took about 10 ns to establish steady heat flow and an additional 50–500 ns for averaging the temperature profile and heat flux, depending on the system size.

Since the classical molecular dynamics is not valid for the system temperature below the Debye temperature, quantum corrections must be applied to the temperature and the thermal conductivity predicted by the MD simulations. We considered the quantum effect in the reported EMD and NEMD results according to the following expression [35]

$$T_{MD} = \frac{1}{k_B}\int_0^{\nu_{\max}} D(\nu)\left[\frac{1}{\exp(h\nu/k_B T_{qc})-1}+\frac{1}{2}\right]h\nu d\nu, \tag{6}$$

where ν is phonon frequency; $D(\nu)$ is the normalized vibrational density of states (VDOS) of silicene calculated by taking the Fourier transform of the atomic velocity autocorrelation function (VACF) from the MD simulation [36]; $\nu_{\max}$ is the maximal phonon frequency of VDOS; $1/[\exp(h\nu/k_B T_{qc})-1]$ is the Bose-Einstein distribution and h is the Planck constant; $d\nu$ is the minimum frequency interval of VDOS; and T_{MD} and T_{qc} are the MD and quantum-corrected temperature, respectively. In our simulation, T_{qc} is calculated to be 230 K for $T_{MD} = 300$ K. The quantum-corrected thermal conductivity is calculated by [37]

$$\kappa_{qc} = \kappa_{\mathrm{MD}}\frac{\partial T_{\mathrm{MD}}}{\partial T_{qc}}. \tag{7}$$

The results of the in-plane thermal conductivity of silicene calculated by EMD and NEMD using the optimized SW1 and optimized SW2 parameters are reported in Fig. 3. Note that we only used the optimized SW1 parameters for EMD calculations. We first notice that the size effect of the thermal conductivity of silicene from EMD simulation with the optimized SW1 parameters is minimal, and it stabilizes around 5.5 W/mK for all sizes considered. In addition, the thermal conductivity in the zigzag and armchair directions does not show any difference. However, for the NEMD results, there is a significant length dependence in the thermal conductivity. The thermal conductivity increases rapidly with the silicene length below 300 nm and then increases very slowly when the length becomes longer. The thermal conductivity of the infinitely long silicene (κ_∞) and the effective phonon mean-free path (MFP, l) were obtained by fitting the data using the equation [30]

$$\frac{1}{\kappa_{qc}} = \frac{1}{\kappa_\infty}\left(\frac{l}{L_y}+1\right). \tag{8}$$

It is worth pointing out that we only used the data with the silicene length longer than 80 nm to fit Eq. (8) because the system size used for fitting should be much larger than the phonon MFP to avoid an unphysical prediction for κ_∞, as suggested in a previous study [38]. Finally we obtained $\kappa_\infty = 8.64$ W/mK and $l = 23.76$ nm for the optimized SW1 parameters and $\kappa_\infty = 11.77$ W/mK and $l = 17.94$ nm for the optimized SW2 parameters. We did not find a more significant increase in κ_∞ for the optimized SW2 parameters than that for the optimized SW1 parameters. Note that both κ_∞ and l are functions of the lattice orientation and temperature. Hence, the obtained value only corresponds to the case of silicene along the zigzag direction at 230 K.

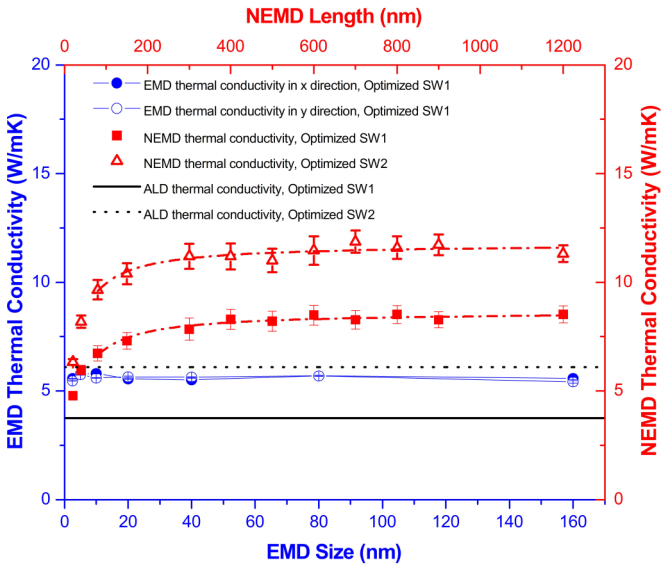

FIG. 3. (Color online) The thermal conductivity of silicene as a function of sample size. The left/bottom and right/top axes correspond to the result calculated by EMD and NEMD simulations, respectively. All results correspond to the real system temperature of 230 K after quantum correction. The black solid and dotted lines are the ALD results at the same temperature for the optimized SW1 and optimized SW2 parameters, respectively. The red dash-dotted lines are the curves fitting to Eq. (8).

We also noticed that the results for the EMD and NEMD methods are not the same, even if we have extrapolated the thermal conductivity to infinitely long for the NEMD simulation. Actually, this is a general issue existing in calculations of the thermal conductivity using the classical molecular dynamics simulation [39]. Nevertheless, from both EMD and NEMD results, we can confirm that the thermal conductivity of silicene is extremely low, which is around 20 times less than the value of bulk silicon (~150 W/mK from experiments) and is comparable to that of silicon nanowires [40–42]. The exceptionally low thermal conductivity makes silicene a promising candidate for thermoelectrics.

We further calculate the thermal conductivity of silicene using the single-mode relaxation time (SMRT) model derived from Boltzmann transport equation

$$\kappa = \sum_p c_p \upsilon_{g,p}^2 \tau_p, \tag{9}$$

where c is the heat capacity, υ_g is group velocity, τ is the phonon relaxation time, and the subscript p goes over all phonon modes in this system. The group velocities of phonons are calculated using a central difference method, and phonon relaxation time values are obtained using ALD. The ALD method calculates the scattering rates of all the three-phonon processes from the anharmonic force constants, which are obtained by a finite difference method with a silicene supercell with 60 atoms. The details of ALD can be found in

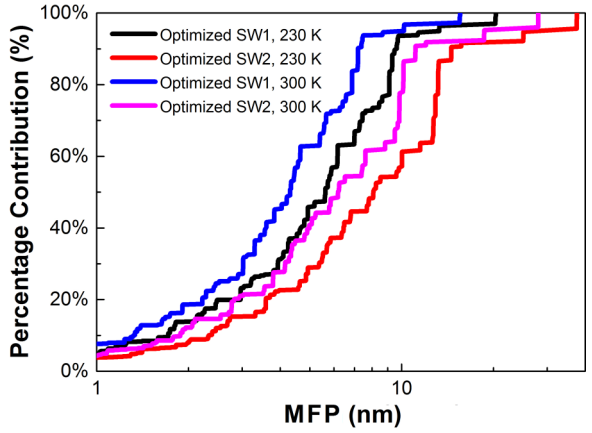

FIG. 4. (Color online) The percentage contribution to thermal conductivity as a function of phonon MFP for the optimized SW1 and optimized SW2 parameters at 230 and 300 K.

other references [43–45] and will not be presented here. It is generally believed that only Umklapp phonon scattering process will contribute to thermal resistance, so there are suggestions that only Umklapp process should be considered when the relaxation time is calculated. However, it was noticed that if only Umklapp process were considered, the thermal conductivity would be significantly overestimated using the SMRT model, because the normal process can help populate the long wavelength modes that carries the majority of the heat [46]. Here, both normal and Umklapp phonon-phonon scattering processes are included when calculating the phonon relaxation time τ, as was the case for most ALD calculations [43–45,47]. The interactions of silicon atoms are described by our optimized SW potentials, and the single-point energies are calculated using the LAMMPS package [29]. Since the SW parameters have a relatively short cutoff, we considered a 7-Å cutoff for harmonic force constants and 5-Å cutoff (third nearest neighbor) for anharmonic force constants. For Brillouin zone integration, we considered a 16 × 16 grid of wave vectors. The thermal conductivity values at 300 K predicted using Eq. (9) are 3.33 W/mK for the optimized SW1 parameters and 5.43 W/mK for the optimized SW2 parameters. To compare with the MD results with quantum correction, we also evaluated the thermal conductivity values at 230 K, which are 3.75 W/mK for the optimized SW1 parameters and 6.11 W/mK for the optimized SW2 parameters. These values are shown in Fig. 3 for comparison with MD results. The thermal conductivity calculated by ALD is smaller than those from MD simulations. The discrepancy is mainly attributed to the strong normal scattering near the zone center in two-dimensional materials, as also seen in graphene [46].

IV. CONTRIBUTIONS OF DIFFERENT MODES AND DIRECTIONAL VIBRATIONS

Anharmonic lattice dynamics allows us to determine the mode-specific contributions to thermal conductivity. Therefore, we plot the percentage contribution to thermal conductivity as a function of phonon MFP, as shown in Fig. 4. We can see that the phonon MFP smaller than 10 nm actually contributes to almost 80% of the total thermal conductivity for the optimized SW1 parameters and about 50% for the optimized SW2 parameters. No matter which potential is considered, this value is much smaller than the case of bulk silicon, for which the representative phonon MFP is about 1 μm at 300 K [44]. Note that the MFP calculated by ALD is a little smaller than that obtained from NEMD results, which is probably due to the difference in definitions.

Our ALD calculations predict that the phonon modes of silicene with a wavelength less than 10 nm contribute more than 50% of the overall thermal conductivity. However, this does not imply that the NEMD process can converge in a few nanometers. From Fig. 3, we can see that the thermal conductivity of silicene calculated by NEMD converges at about 300 nm, because MFP is not the only factor that is important to the NEMD simulation size. Wavelength is also a concern. A larger system has longer wavelength phonons. These phonons may not contribute much to the heat conduction by carrying heat themselves, but they contribute a great deal to the heat conduction process by scattering with other phonons. Therefore, to include these long wavelength phonons is also important to the convergence of the NEMD process. A previous study on Lennard-Jones argon also shows that the NEMD process usually converges at a length one order of magnitude larger than the bulk MFP [43]. The same phenomena have been found in other low-dimensional systems [48–50].

Another interesting question is how much the out-of-plane flexural (or ZA) modes contribute to the thermal conductivity. In graphene, it is known that ZA mode has a major contribution to its high thermal conductivity [51]. However, since silicene has a buckled structure, the normal modes cannot be categorized into pure out-of-plane or in-plane modes. We have observed that the eigenvectors corresponding to the quadratic phonon branch in Fig. 2 contains both in-plane and out-of-plane vibrations, so they are not pure ZA modes (we will see details later). Nevertheless, we quantify the relative contributions of lattice vibrations in the x, y, and z directions to the total heat flux of silicene, by using the NEMD-based method we proposed recently [5,50,52,53]

$$J_{A\to B,\alpha} = -\frac{1}{2S}\sum_{i\in A}\sum_{j\in B} F_{ij\alpha}(\upsilon_{i\alpha}+\upsilon_{j\alpha}), \qquad (10)$$

where α is x, y, or z direction, A and B are the left and right side of a virtual interface located at the middle of silicene in the y direction, $J_{A\to B,\alpha}$ is the heat flux from A to B due to lattice vibrations in α direction, S is the cross-sectional area, $F_{ij\alpha}$ is the α component of the force acting on atom i due to atom j, and $\upsilon_{i\alpha}$ is the α component of the velocity of atom i. Although the above formula is based on two-body interactions and the SW potential used is a three-body potential, it has been demonstrated that the three-body forces can be decomposed into two-body components [5,52]. We have verified that the long-time average heat flux calculated by Eq. (10) is technically equal to J_L in Eq. (5). The directional contribution (percentage) to the total heat flux for different lengths of silicene is compared in Fig. 5. It is clearly seen that for all lengths of silicene, as much as 80% of the total heat flux is contributed by the lattice vibration in the y direction (i.e., the longitudinal modes). The lattice vibration in the

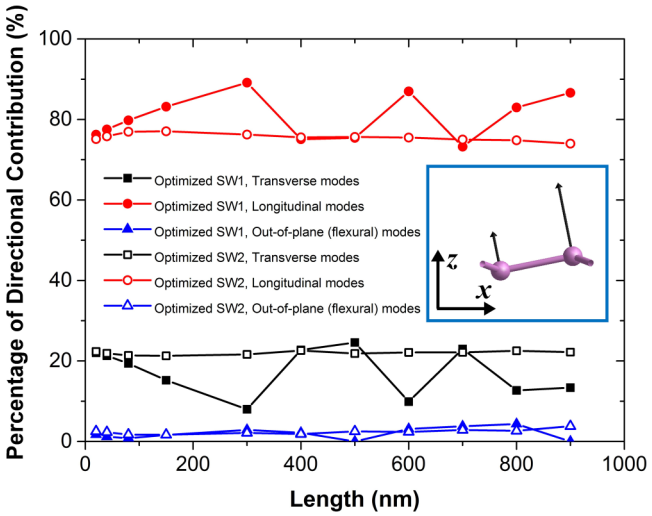

FIG. 5. (Color online) Relative contribution (percentage) of lattice vibrations in the x (transverse), y (longitudinal), and z (out-of-plane) directions to total heat flux in the NEMD simulation. Inset: atomic displacements of a typical out-of-plane acoustic (ZA) phonon mode in silicene at the M-point of the first Brillouin zone.

x direction (i.e., the in-plane transverse modes) takes the remaining 20%, and the lattice vibration in the z direction (i.e., the out-of-plane flexural modes) contributes nearly zero. This behavior is fundamentally different from graphene, where the out-of-plane flexural acoustic modes dominate (~70%) the thermal transport [5,51]. The weak contribution of the out-of-plane flexural phonon modes can be attributed to two combined aspects: (1) the main reason is anticipated to be the buckling structure in silicene, which leads to strong coupling between out-of-plane modes and in-plane modes; and (2) the bonding strength of Si-Si bonds is much weaker as compared with C-C bonds in graphene, which leads to a significantly lower group velocity of the ZA modes in silicene. It is worth pointing out that such a difference in the mode-specific contribution is expected from the different atomic structure between silicene and graphene (buckled vs planar), as the buckled structure of silicene implies that the ZA modes may behave differently in silicene than in graphene; therefore, the negligible ZA contribution to the overall phonon transport in silicene is understandable. In fact, we have observed that a considerable amount of the ZA phonon modes in silicene are not pure flexural modes. In the inset of Fig. 5, we show the atomic displacements of a typical ZA phonon mode at the M point of the first Brillouin zone. We can clearly see that the base atoms do not exactly vibrate along the out-of-plane (z) direction, instead there is an in-plane (x) component, i.e., TA mode, coupled with the flexural mode. Such coupling is the general case for ZA modes with the k-point along $\Gamma \rightarrow M$. We also found that the LA modes couple with other modes for k-point along $\Gamma \rightarrow K \rightarrow M$. The strong coupling between the out-of-plane flexural modes and the in-plane transverse modes could hinder the heat conduction carried by the ZA modes, which leads to the negligible contribution of ZA modes to the overall phonon transport, shown in Fig. 5.

V. SUMMARY AND CONCLUSION

In summary, we have optimized SW parameters for silicene, and the new parameters successfully reproduce the low buckling structure of silicene and the phonon dispersion curves from *ab initio* calculations. We then calculated the thermal conductivity of silicene by both EMD and NEMD simulations, as well as the ALD method. The mode-specific contribution to lattice thermal conductivity is analyzed using the ALD method, and we found that the thermal conductivity of silicene is mainly contributed by phonons with MFP smaller than 10 nm, which is quite different from bulk silicon. Moreover, by qualifying the relative contributions of lattice vibrations in different directions, we found that the longitudinal phonon modes dominate the thermal transport in silicene, which is fundamentally different from graphene, despite the similarity of their two-dimensional honeycomb lattices. We expect that our new optimized SW potential will arouse great interest in investigating the physical properties of silicene using the classical molecular dynamics simulation.

ACKNOWLEDGMENTS

This work is partly supported by the National Natural Science Foundation of China (No. 51306111) and Shanghai Municipal Natural Science Foundation (No. 13ZR1456000). X.Z. would like to thank Z. Fan for helpful discussions about the parameter fitting using the GULP program. Simulations were performed with computing resources granted by the Jülich Aachen Research Alliance-High Performance Computing (JARA-HPC) from RWTH Aachen University under Project No. jara0073, HPC from Shanghai Jiao Tong University (π), the Supercomputing Center of Chinese Academy of Sciences (DeepComp 7000), and Shanghai Supercomputer Center (MagicCube). This work is also supported in part by the Ministry of Science and Technology of China (Grants No. 2012 CB932900 and No. 2013CB933401) and the Chinese Academy of Sciences.

[1] K. S. Novoselov, V. I. Fal'ko, L. Colombo, P. R. Gellert, M. G. Schwab, and K. Kim, Nature (London) **490**, 192 (2012).
[2] A. Kara, H. Enriquez, A. P. Seitsonen, L. C. Lew Yan Voon, S. Vizzini, B. Aufray, and H. Oughaddou, Surf. Sci. Rep. **67**, 1 (2012).
[3] P. Vogt, P. De Padova, C. Quaresima, J. Avila, E. Frantzeskakis, M. C. Asensio, A. Resta, B. Ealet, and G. Le Lay, Phys. Rev. Lett. **108**, 155501 (2012).
[4] B. Huang, H. J. Xiang, and S.-H. Wei, Phys. Rev. Lett. **111**, 145502 (2013).
[5] M. Hu, X. Zhang, and D. Poulikakos, Phys. Rev. B **87**, 195417 (2013).
[6] J. Chen, C. Jang, S. Xiao, M. Ishigami, and M. S. Fuhrer, Nat. Nanotechnol. **3**, 206 (2008).
[7] A. A. Balandin, S. Ghosh, W. Bao, I. Calizo, D. Teweldebrhan, F. Miao, and C. N. Lau, Nano Lett. **8**, 902 (2008).

[8] J. H. Seol, I. Jo, A. L. Moore, L. Lindsay, Z. H. Aitken, M. T. Pettes, X. Li, Z. Yao, R. Huang, D. Broido, N. Mingo, R. S. Ruoff, and L. Shi, Science **328**, 213 (2010).

[9] S. Lebègue and O. Eriksson, Phys. Rev. B **79**, 115409 (2009).

[10] K. Zberecki, M. Wierzbicki, J. Barnaś, and R. Swirkowicz, Phys. Rev. B **88**, 115404 (2013).

[11] D. Jose and A. Datta, Phys. Chem. Chem. Phys. **13**, 7304 (2011).

[12] G. A. Tritsaris, E. Kaxiras, S. Meng, and E. Wang, Nano Lett. **13**, 2258 (2013).

[13] C. J. Tabert and E. J. Nicol, Phys. Rev. Lett. **110**, 197402 (2013).

[14] L. Meng, Y. Wang, L. Zhang, S. Du, R. Wu, L. Li, Y. Zhang, G. Li, H. Zhou, W. A. Hofer, and H. Gao, Nano Lett. **13**, 685 (2013).

[15] T. H. Osborn, A. A. Farajian, O. V. Pupysheva, R. S. Aga, and L. C. Lew Yan Voon, Chem. Phys. Lett. **511**, 101 (2011).

[16] F. H. Stillinger and T. A. Weber, Phys. Rev. B **31**, 5262 (1985).

[17] B. Qiu, H. Bao, G. Zhang, Y. Wu, and X. Ruan, Comput. Mater. Sci. **53**, 278 (2012).

[18] J. Tersoff, Phys. Rev. B **39**, 5566 (1989).

[19] J. Tersoff, Phys. Rev. B **41**, 3248 (1990).

[20] P. Giannozzi, S. Baroni, N. Bonini, M. Calandra, R. Car, C. Cavazzoni, D. Ceresoli, G. L. Chiarotti, M. Cococcioni, I. Dabo, A. D. Corso, S. de Gironcoli, S. Fabris, G. Fratesi, R. Gebauer, U. Gerstmann, C. Gougoussis, A. Kokalj, M. Lazzeri, L. Martin-Samos *et al.*, J. Phys.: Condens. Matter **21**, 395502 (2009).

[21] J. P. Perdew and A. Zunger, Phys. Rev. B **23**, 5048 (1981).

[22] D. R. Hamann, M. Schlüter, and C. Chiang, Phys. Rev. Lett. **43**, 1494 (1979).

[23] S. Cahangirov, M. Topsakal, E. Aktürk, H. Şahin, and S. Ciraci, Phys. Rev. Lett. **102**, 236804 (2009).

[24] Z. Ni, Q. Liu, K. Tang, J. Zheng, J. Zhou, R. Qin, Z. Gao, D. Yu, and J. Lu, Nano Lett. **12**, 113 (2012).

[25] B. Lalmi, H. Oughaddou, H. Enriquez, A. Kara, S. Vizzini, B. Ealet, and B. Aufray, Appl. Phys. Lett. **97**, 223109 (2010).

[26] N. D. Drummond, V. Zólyomi, and V. I. Fal'ko, Phys. Rev. B **85**, 075423 (2012).

[27] S. Baroni, S. de Gironcoli, A. D. Corso, and P. Gianozzi, Rev. Mod. Phys. **73**, 515 (2001).

[28] J. D. Gale, J. Chem. Soc. Faraday Trans. **93**, 629 (1997).

[29] S. Plimpton, J. Comput. Phys. **117**, 1 (1995).

[30] P. K. Schelling, S. R. Phillpot, and P. Keblinski, Phys. Rev. B **65**, 144306 (2002).

[31] S. Nosé, J. Chem. Phys. **81**, 511 (1984).

[32] W. G. Hoover, Phys. Rev. A **31**, 1695 (1985).

[33] P. Jund and R. Jullien, Phys. Rev. B **59**, 13707 (1999).

[34] F. Müller-Plathe, J. Chem. Phys. **106**, 6082 (1997).

[35] C. Z. Wang, C. T. Chan, and K. M. Ho, Phys. Rev. B **42**,11276 (1990).

[36] J. M. Dickey and A. Paskin, Phys. Rev. **188**, 1407 (1969).

[37] Y. H. Lee, R. Biswas, C. M. Soukoulis, C. Z. Wang, C. T. Chan, and K. M. Ho, Phys. Rev. B **43**, 6573 (1991).

[38] X. W. Zhou, S. Aubry, R. E. Jones, A. Greenstein, and P. K. Schelling, Phys. Rev. B **79**, 115201 (2009).

[39] Y. He, I. Savić, D. Donadio, and G. Galli, Phys. Chem. Chem. Phys. **14**, 16209 (2012).

[40] D. Li, Y. Wu, P. Kim, L. Shi, P. Yang, and A. Majumdar, Appl. Phys. Lett. **83**, 2934 (2003).

[41] N. Mingo, Phys. Rev. B **68**, 113308 (2003).

[42] S. G. Volz and G. Chen, App. Phys. Lett. **75**, 2056 (1999).

[43] J. E. Turney, E. S. Landry, A. J. H. McGaughey, and C. H. Amon, Phys. Rev. B **79**, 064301 (2009).

[44] K. Esfarjani, G. Chen, and H. T. Stokes, Phys. Rev. B **84**, 085204 (2011).

[45] H. Bao, Acta Phys. Sin. **62**, 186302 (2013).

[46] D. Singh, J. Y. Murthy, and T. S. Fisher, J. Appl. Phys. **110**, 094312 (2011).

[47] W. Li, J. Carrete, and N. Mingo, Appl. Phys. Lett. **103**, 253103 (2013).

[48] M. Hu, X. Zhang, K. P. Giapis, and D. Poulikakos, Phys. Rev. B **84**, 085442 (2011).

[49] M. Hu and D. Poulikakos, Nano Lett. **12**, 5487 (2012).

[50] Y. Jing, M. Hu, and L. Guo, J. Appl. Phys. **114**, 153518 (2013).

[51] L. Lindsay, D. A. Broido, and N. Mingo, Phys. Rev. B **82**, 115427 (2010).

[52] X. Zhang, M. Hu, and D. Tang, J. Appl. Phys. **113**, 194307 (2013).

[53] X. Zhang and J. Jiang, J. Phys. Chem. C **117**, 18441 (2013).